ORIGINAL ARTICLE

Rock slope stability assessment based on the critical failure state curve for the generalized Hoek−Brown criterion

Wenlian Zhang[1,2] · Xiaoyun Sun[1,3] · Wei Yuan[2] · Ting Liu[1] · Shenyi Jin[2]

Abstract

The strength reduction method (SRM) based on the generalized Hoek−Brown (GHB) criterion has become an important and popular topic to analyse the stability of rock slopes. Various reduction strategies have been proposed and applied by the civil and mining engineering community. This paper proposed a new SRM for rock slopes with the GHB criterion based on the critical failure state curve (CFSC). The existence of the CFSC has been proven by theoretical analysis, and the explicit expression of the CFSCs for different parameters m_i and slope angles β, considering the influence of disturbance factor D, has been obtained by curve fitting based on a great deal of simulation data. The new SRM provides a graphic method to determine the parameters at the critical failure state from the initial state by reducing the compressive strength of intact rock σ_{ci} and the parameter combination s^α with the same ratio and proposes a definition of the factor of safety (FOS) based on the parameters of the two states. This method was applied to nine slope examples to verify its validity and accuracy. The relative errors between the critical state parameters obtained from the graphic method and that from the simulation analysis are less than 10%, which proves the accuracy of the CFSCs. The FOSs obtained by the proposed definition are compared with those obtained by the Bishop simplified method and the local linearization method (LLM), and the results are very close. The relative error is less than $\pm 5\%$ compared with the LLM, and the stability state predicted is perfectly accurate. However, the calculation procedure is largely simplified, and the calculation speed is largely improved. A practical case of an open pit limestone slope with multiple steps was detailed analysed by the proposed SRM based on CFSC. The FOS results comparison with other existing method has demonstrated its feasibility and reliability in engineering application.

✉ Xiaoyun Sun
  sunxy1971@126.com

  Wenlian Zhang
  wenlian_zhang1112@163.com

[1] School of Electric and Electronic Engineering, Shijiazhuang Tiedao University, Shijiazhuang 050043, China

[2] School of Civil Engineering, Shijiazhuang Tiedao University, Shijiazhuang 050043, China

[3] Hebei Provincial Collaborative Innovation Center of Transportation Power Grid Intelligent Integration Technology and Equipment, Shijiazhuang Tiedao University, Shijiazhuang 050043, China

Introduction

The stability assessment and analysis of rock slopes is a significant task for rock engineering projects, such as open pit mining. The strength reduction method (SRM) is widely accepted and used by researchers to analyse slope stability because of its advantage over the traditional limit equilibrium method (LEM) (Zhao et al. 2005; Krahn 2007; Liu et al. 2015; Sari 2019). Presently, SRM research is mainly based on the conventional Mohr−Coulomb (MC) criterion, which is incapable of explaining the nonlinear deformation and failure characteristics of rock masses. The Hoek−Brown (HB) criterion, first proposed in 1980 as an empirical nonlinear failure criterion, has developed into a rigorous and complete strength criterion and has been widely applied in rock mechanics and engineering (Hoek and Brown 1980; Hoek et al. 2002). The Generalized Hoek−Brown (GHB)

criterion, as the latest version of the HB criterion presented in 2018 (Hoek and Brown 2019), is capable of estimating the strength and deformation characteristics of homogeneous and isotropic rocks with few discontinuities and heavily jointed rock masses. Combining the advantage of SRM on slope stability analysis and the nonlinear GHB criterion to explore the new strength reduction strategy has become an important and popular research field (Zong and Xu 2008; Melkoumian et al. 2009; Shen and Karakus 2014; Yuan et al. 2020). Due to the complexity of the parameters in the GHB criterion, various reduction strategies have been proposed and applied by many scholars, but none of them has gained wide acceptance in the engineering community. Presently, the representative reduction methods are classified into the following four types:

(1)   Some or all of the GHB parameters are directly reduced by the reduction factor is usually called the "direct reduction method", and the global safety factor is traditionally defined by the reduction ratio of the original parameters to the reduced parameters at failure. For example, Wu et al. (2006) suggested reducing the uniaxial compressive strength of the intact rock (σ_{ci}) and the material constant for the intact rock (m_i) with the same ratio. Han et al. (2016) presented the correlation between the three reduction factors of the parameters (*mb, s, a*) in Hoek–Brown criterion from the softening and hardening regularities of the geomaterial perspective. Song et al. (2012) discussed seven cases of the direct reduction method and found that directly reducing σ_{ci} and the geological strength index (*GSI*) could obtain a reasonable global safety factor. However, the direct reduction method could lead to distortion of the GHB failure envelope after the parameters are reduced.

(2)   The integral strength envelope of the GHB criterion is lowered by a reduction factor until the critical failure state, as proposed by Hammah et al. (2005). The determination of the equivalent GHB curve that best approximates the lowered envelope is obtained through the minimization of the total squared error by the simplex method, of which the analysis procedure is complex. Thomas et al. (2008) adopted the spatial mobilized plane (SMP) concept to realize intrinsic material strength factorization. However, this method requires iterative computations to obtain the shear strength at every reduction step, which greatly lowers the calculation efficiency.

(3)   The nonlinear GHB criterion is transformed into the linear MC criterion, and the slope stability is analysed based on the MC criterion, called the equivalent linearization method (Priest 2005; Yang and Yin 2010; Shen et al. 2012). This method was classified into two types: the global approach (Hoek et al. 2002; Zong and Xu 2008) and the local approach (Fu and Liao 2010; Xu and Yang 2018; Wei et al. 2021). The former is to obtain a global linear optimization of the shear strength curve of the GHB criterion; the latter is to obtain the local stress and strength values. Sukanya et al. (2012) believed that the local approach was physically more correct than the global approach. However, the local MC parameters need to be solved by the Newton iterative formula, and the calculation is time-consuming for a complex model.

(4)   Applying stability charts for rock mass slopes satisfying the HB criterion to obtain the safety factor of the slope (Li et al. 2008; Shen et al. 2013; Sun et al. 2016). For example, Shen et al. (2013) and Sun et al. (2016) proposed a slope stability chart for a specified slope angle $\beta = 45°$ and disturbance factor $D = 0$ and then combined the weighting factors f_D and f_β to calculate the FOS of a slope assigned various slope angles under different blasting damage. The graph method relies heavily on the accuracy of chart data.

Recently, a new SRM strategy based on the GHB criterion (Yuan et al. 2020), whose core concept is to search for an optimal reduction pathway for the GHB criterion parameters by establishing the critical failure state curves (CFSC) for different slopes. Inspired by its strategy, this paper establishes a more accurate and detailed critical failure state curve equation based on a large amount of numerical simulation data, and an improved parameter reduction scheme and a simpler safety factor definition method are proposed and formed a new SRM based on CFSC. The new SRM allows for rapid determination of the parameters at the critical failure state by a graphic method and a fast and accurate calculation method for the factor of safety (FOS) based on the initial and critical states' parameters. The advantages of the proposed method over those existing SRMs are that the model establishment and stability numerical analysis based on finite element or finite difference programme which consumes significant computational power and time are not required.

The proposed method is applied to several classical examples to verify the validity and reliability of the parameter reduction scheme and the definition of the safety factor. A practical case of an open pit limestone slope with multiple steps was detailed analyzed by the proposed graphical method to demonstrate its feasibility and reliability in engineering application.

The general Hoek–Brown criterion and the slope critical failure state curve

The general Hoek−Brown criterion

The GHB strength criterion is usually given in principal stress space with the following expression.

$$\sigma_1 = \sigma_3 + \sigma_{ci}\left(m_b\frac{\sigma_3}{\sigma_{ci}} + s\right)^{\alpha}, \tag{1}$$

where σ_1 and σ_3 are the maximum and minimum principal stresses of the rock mass at failure (compressive stress is taken to be positive), and σ_{ci} is the unconfined compressive strength of the intact rock according to the 2018 edition (Hoek and Brown 2019). m_b, s, and α are empirical parameters reflecting rock mass characteristics related to the fracturing degree of the rock and can be estimated by the functions of the geological strength index (GSI), the disturbance factor D and the material constant of intact rock mi.

$$\begin{cases} m_b = m_i \exp\left(\frac{\text{GSI}-100}{28-14D}\right) \\ s = \exp\left(\frac{\text{GSI}-100}{9-3D}\right) \\ \alpha = \frac{1}{2} + \frac{1}{6}(e^{-\text{GSI}/15} - e^{-20/3}) \end{cases}, \tag{2}$$

where GSI is estimated by the structure (or blockiness) and the surface conditions of the jointed blocky rock masses, of which the maximum value is 100 (for intact rock). D is the disturbance factor subjected to blasting damage and stress relaxation of the rock mass, with a value range of 0.0 (undisturbed) ~ 1.0 (disturbed). m_i is a material constant for the intact rock, which represents the rock type and hardness.

Balmer (1952) proposed that normal stress and shear stress could be expressed as functions of principal stresses as follows:

$$\begin{cases} \sigma_n = \sigma_3 + \frac{\sigma_1 - \sigma_3}{\partial\sigma_1/\partial\sigma_3 + 1} \\ \tau = (\sigma_1 - \sigma_3)\frac{\sqrt{\partial\sigma_1/\partial\sigma_3}}{\partial\sigma_1/\partial\sigma_3 + 1} \end{cases}. \tag{3}$$

The differential expression $\partial\sigma_1/\partial\sigma_3$ can be derived from Eq. (1) as follows:

$$\partial\sigma_1/\partial\sigma_3 = 1 + \alpha m_b\left(m_b\frac{\sigma_3}{\sigma_{ci}} + s\right)^{\alpha-1}. \tag{4}$$

The expressions of normal stress and shear stress based on the GHB criterion can be obtained by substituting Eqs. (4) into (3), given as follows:

$$\begin{cases} \sigma_n = \sigma_3 + \frac{\sigma_{ci}\left(m_b\frac{\sigma_3}{\sigma_{ci}}+s\right)^{\alpha}}{2+\alpha m_b\left(m_b\frac{\sigma_3}{\sigma_{ci}}+s\right)^{\alpha-1}} \\ \tau = \sigma_{ci}\left(m_b\frac{\sigma_3}{\sigma_{ci}}+s\right)^{\alpha}\frac{\sqrt{1+\alpha m_b\left(m_b\frac{\sigma_3}{\sigma_{ci}}+s\right)^{\alpha-1}}}{2+\alpha m_b\left(m_b\frac{\sigma_3}{\sigma_{ci}}+s\right)^{\alpha-1}} \end{cases}. \tag{5}$$

As noted in the GHB criterion, the uniaxial compressive strength of the rock mass (σ_{cmass}) is expressed by setting $\sigma_3 = 0$, and the tensile strength of the rock mass (σ_{tmass}) can be obtained by setting $\sigma_1 = \sigma_3 = \sigma_{tmass}$, given below:

$$\begin{cases} \sigma_{cmass} = \sigma_{ci}s^{\alpha} \\ = \sigma_{ci}\exp\left(\left(\frac{\text{GSI}-100}{9-3D}\right)\left(\frac{1}{2}+\frac{1}{6}(e^{-\text{GSI}/15}-e^{-20/3})\right)\right) \\ \sigma_{tmass} = -s\frac{\sigma_{ci}}{m_b} \end{cases}. \tag{6}$$

Theoretical relationships of slope parameters at the critical failure state

The stability of the slope is determined by the unit weight of the rock mass (γ), the slope height (H), the slope angle (β) and all the parameters involved in the failure criterion of the rock mass. Based on the GHB criterion, a general functional relationship related to all the parameters to describe the critical failure state of any slope could be established. According to the classic definition of the factor of safety (FOS), a slope at the critical failure state indicates an equilibrium between the total resistant shear force and the total sliding force on the potential sliding surface. Thus, this equilibrium state for any slope can be deduced as follows:

$$F = \frac{\int_l \tau_s dl}{\int_l \tau_m dl} = f_1\left(\frac{\tau_s}{\tau_m}\right) = 1, \tag{7}$$

where l denotes the potential sliding surface; in each zone, τ_s is the resistant shear stress; and τ_m is the driving shear stress, which greatly depends on the gravity of the overlying rock mass above the potential sliding surface (γH). Thus, Eq. (7) can be expressed as:

$$f_2\left(\frac{\tau_s}{\gamma H}\right) = 1. \tag{8}$$

From the formula in Eq. (5), the following equation can be derived.

$$\begin{cases} \frac{\sigma_n}{\sigma_{ci}} = \frac{\sigma_3}{\sigma_{ci}} + \frac{\left(m_b\frac{\sigma_3}{\sigma_{ci}}+s\right)^{\alpha}}{2+\alpha m_b\left(m_b\frac{\sigma_3}{\sigma_{ci}}+s\right)^{\alpha-1}} \\ \frac{\tau_s}{\sigma_{ci}} = \left(m_b\frac{\sigma_3}{\sigma_{ci}}+s\right)^{\alpha}\frac{\sqrt{1+\alpha m_b\left(m_b\frac{\sigma_3}{\sigma_{ci}}+s\right)^{\alpha-1}}}{2+\alpha m_b\left(m_b\frac{\sigma_3}{\sigma_{ci}}+s\right)^{\alpha-1}} \end{cases}. \tag{9}$$

Therefore, the minor principal stress σ_3/σ_{ci} can be solved by an iteration of σ_n/σ_{ci} with given m_b, s and α. τ/σ_{ci} is the function of σ_3/σ_{ci}, m_b, s and α. Thus, τ/σ_{ci} can be expressed as follows:

$$\frac{\tau_s}{\sigma_{ci}} = f_3\left(\frac{\sigma_n}{\sigma_{ci}}, m_b, s, \alpha\right). \tag{10}$$

The value of σ_n depends on the gravity of the overlying rock mass γH and the slope angle β only under the condition of gravity. Thus, Eq. (10) can be expressed as:

$$\frac{\tau_s}{\sigma_{ci}} = f_4\left(\frac{\gamma H}{\sigma_{ci}}, \beta, m_b, s, \alpha\right), \tag{11}$$

where the parameters m_b, s and α can be expressed by Eq. (2). Thus, Eq. (11) can be expressed as follows:

$$\tau_s = \sigma_{ci} f_5\left(\frac{\gamma H}{\sigma_{ci}}, \beta, GSI, D, m_i\right). \tag{12}$$

According to the equilibrium criterion in Eq. (8), the expression below can be derived:

$$f_2\left(\frac{\tau_s}{\gamma H}\right) = f_2\left(\frac{\sigma_{ci}}{rH} f_5\left(\frac{\gamma H}{\sigma_{ci}}, \beta, GSI, D, m_i\right)\right)$$
$$= f_6\left(\frac{\sigma_{ci}}{\gamma H}, GSI, D, m_i, \beta\right) = 1. \tag{13}$$

According to Eq. (6), s^α is the function of GSI and D. Thus, Eq. (13) is finally expressed as:

$$f_7\left(\frac{\sigma_{ci}}{\gamma H}, s^\alpha, m_i, \beta\right) = 1. \tag{14}$$

In the literature of Yuan et al.(2020), σ_{ci} and s^α are combined and replaced by σ_{cmass} from Eq. (6). In addition, Eq. (14) is deduced below.

$$f_7\left(\frac{\sigma_{ci}}{\gamma H}, s^\alpha, m_i, \beta\right) = f_8\left(\frac{\sigma_{ci}s^\alpha}{\gamma H}, m_i, \beta\right) = f_7(\lambda, \beta, m_i) = 1, \tag{15}$$

where $\lambda = \frac{\sigma_{ci}s^\alpha}{\gamma H}$ is a dimensionless parameter. The parameters λ, β and mi, which satisfy the equilibrium criterion in Eq. (15) at the slope critical failure state, could establish the slope critical failure state curve (CFSC).

Explicit expression of the CFSC by numerical simulation

It is a great challenge to establish the explicit expression of CFSC from the implicit function (15) by theoretical analysis. Thus, a numerical simulation method based on FLAC^{3D} 6.0 software (Itasca Inc., 2016) is used to achieve
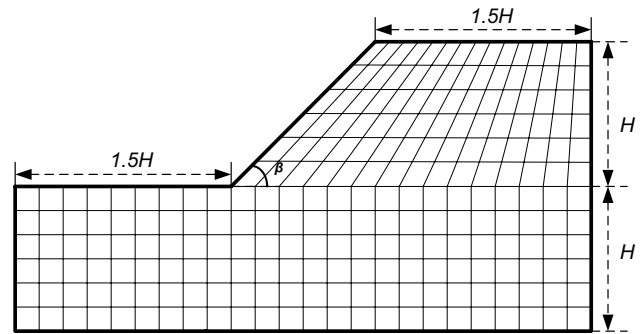

Fig. 1 The geometry and grid layout of the slope model

this goal. Referring to reference (Hammah et al 2005; Fu and Liao 2010), the geometry and grid layout of the slope model used in this numerical simulation is shown in Fig. 1.

To simplify the simulation procedure, the slope angle is assigned to 45°, 60° and 75°. The height of the slope models is assigned to 10 m, 25 m, 50 m, 100 m and 200 m (the heights are fine adjusted in accordance with the slope angles shown in Table 1). The horizontal displacements of the left and right boundaries are fixed, while both horizontal and vertical displacements are fixed along the bottom boundary. The unit weight γ is set to 25.0 kN/m^3. The disturbance factor D is initially set to 0, and its influence on the CFSC is discussed in "The influence of disturbance factor D on the CFSCs". Only the gravity of the rock mass is considered as an external load in the numerical simulation. The convergence criterion to judge whether the slope has reached a mechanically stable state is setting the maximum unbalance force ratio R to 10^{-5}. The slope model was considered to be homogeneous and isotropic. Considering the mesh sensitivity, the amount of grids remains the same for different slope models (approximately 4000~5000 grids).

The elasticity modulus (E) and Poisson's ratio (ν) of the rock mass remain constant when the GSI, D and σ_{ci} vary in this study. Because this study pays more attention to the parameters causing plastic failure than the parameters involved in elastic deformation. The simulation results have proven that the changes in the elastic modulus and Poisson coefficient do not affect the parameters of the slope critical failure state.

Table 1 Slope model and values set for the parameters

Slope angle	Slope height (m)	GSI range	m_i	D
45°	10, 20, 50, 100, 200, 400	3–45	2,5,10,15,20,25	0
60°	17, 34, 51, 204	5–60	5,10,15,20,25	0
75°	37, 74, 222	8–70	5,10,15,20,25	0

The procedure of the numerical simulation is as follows:

(1) Slope models with different slope angles and heights are established, and the rock mass is assigned to be homogeneous and isotropic.

(2) For each slope model, the unit weight of the rock mass remains the same, and the disturbance factor D is initially set to 0. m_i is fixed as the value in Table 1. GSI is varied with the range of Table 1, and finally, σ_{ci} is adjusted to lead the slope to the critical failure state. The material parameter values (m_b, s and α) of the slope model are transformed by the Fish function in FLAC^{3D} with the values of GSI, m_i and D, and σ_{ci} is repeatedly reduced by an interval of 0.2 until the numerical calculation does not converge, which means that the slope has reached the critical failure state.

(3) The uniaxial compressive strength of the rock mass σ_{cmass} and the dimensionless parameter λ are calculated according to the parameters at each critical failure state. The simulation results show that the dimensionless parameter λ at the critical failure state remains constant for different heights and unit weights, while it varies with GSI, m_i and slope angle $β$. Figure 2 shows the critical failure state curve of the dimensionless parameter λ varying with GSI for different vales of m_i and slope angle $β$.

To better represent the theoretical relation, the dimensionless parameter λ can be decomposed as the multiplication of two parameters, $\sigma_{ci}/\gamma H$ and s^α, as shown in Eq. (16), where $\sigma_{ci}/\gamma H$ was termed the strength ratio (SR) of a rock slope and was strongly related to the safety factor, proposed by Shen et al.(2013), and s^α determined by GSI and D, is numerically equivalent to JP(Jointing Parameter) of the Palmström's RMi system (Russo 2008), which represented the rock mass quality and structure.

$$\lambda = \frac{\sigma_{cmass}}{\gamma H} = \frac{\sigma_{ci}}{\gamma H} \cdot s^\alpha, \tag{16}$$

s^α is taken as the x-coordinate, and $\sigma_{ci}/\gamma H$ is taken as the y-coordinate. The points paired by s^α and $\sigma_{ci}/\gamma H$ at the critical failure state for different vales of m_i and slope angles $β$ are drawn in the $s^\alpha \sim \sigma_{ci}/\gamma H$ coordinate system, which forms the slope CFSC.

The Curve Fitting Tool (cftool) of MATLAB (Mathworks Inc. 2010) was used to fit the CFSC. After comparing various fitting methods, it was found that the fitting type power 2 ($a * x^b + c$) had the highest fitting accuracy and the minimal fitting error. The fitting expressions of the CFSCs and fitting accuracy are given in Table 2. The points paired by s^α and $\sigma_{ci}/\gamma H$ at the critical failure state and the fitting curve for different slope angles and values of m_i are shown in Fig. 3.

When mi takes values other than 5, 10, 15, 20 and 25, the corresponding CFSCs can be obtained by interpolation. Since the curve of λ varying with mi does not satisfy the linear relation, the CFSCs of other mi values can be obtained by cubic spline interpolation.

The influence of disturbance factor D on the CFSCs

The value of disturbance factor D has a great influence on slope stability (Li et al. 2011). In the latest version of the GHB criterion, the suggested values of D are given for different engineering slopes, that is, $D = 0.5$ for controlled presplit or smooth wall blasting, $D = 0.7$ for mechanical excavation effects of stress reduction damage, and $D = 1.0$ for production blasting. The influence of D on the CFSCs is presented by setting $D = 0.5$, 0.7, 0.9 and 1.0.

Fixing $β$ and m_i, search for the parameter combination ($s^\alpha \sim \sigma_{ci}/\gamma H$) of the critical failure state for $D = 0.5$, 0.7,
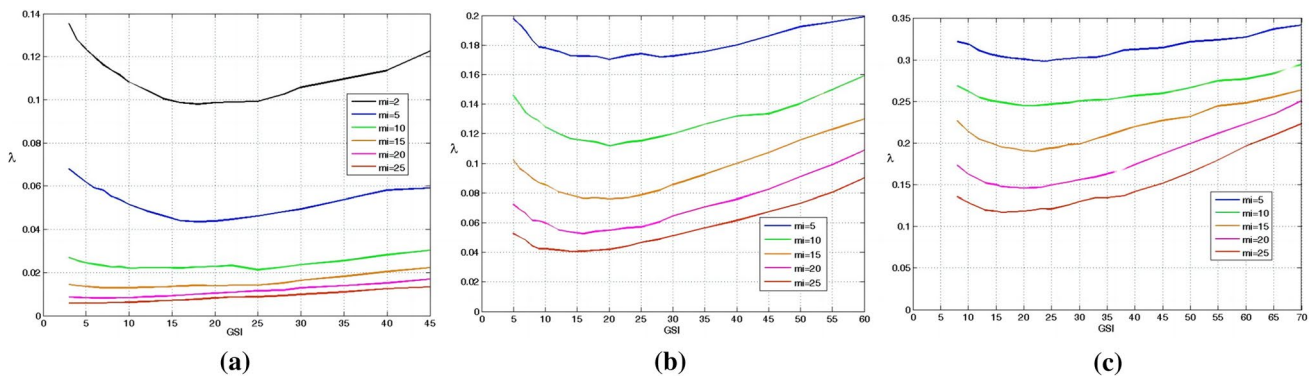

Fig. 2 The critical failure state curve of λ varying with *GSI* for different mi and β

Table 2 The fitting expressions and accuracy of the CFSCs for different m_i and β

Slope angle β	Parameter m_i	Range of GSI	The fitting expression	RMSE [a]	R-square [b]
45°	2	3–45	$y = 0.0268 * x^\wedge(-1.231) + 1.896$	0.2190	1.0000
	5	3~45	$y = 0.007504 * x^\wedge(-1.319) + 1.121$	0.1884	0.9999
	10	3~45	$y = 0.004628 * x^\wedge(-1.251) + 0.7057$	0.2178	0.9992
	15	3~45	$y = 0.004123 * x^\wedge(-1.177) + 0.4800$	0.1146	0.9992
	20	3~45	$y = 0.00394 * x^\wedge(-1.107) + 0.3967$	0.0946	0.9985
	25	3~45	$y = 0.005685 * x^\wedge(-0.9982) + 0.2571$	0.0555	0.9989
60°	5	5~60	$y = 0.07588 * x^\wedge(-1.144) + 1.778$	0.6764	0.9997
	10	5~60	$y = 0.02968 * x^\wedge(-1.239) + 1.913$	0.5715	0.9997
	15	5~60	$y = 0.01425 * x^\wedge(-1.296) + 1.76$	0.4311	0.9996
	20	5~60	$y = 0.007328 * x^\wedge(-1.345) + 1.584$	0.4312	0.9992
	25	5~60	$y = 0.004671 * x^\wedge(-1.364) + 1.459$	0.4967	0.9979
75°	5	8~65	$y = 0.2065 * x^\wedge(-1.071) + 1.228$	0.3656	0.9999
	10	8~65	$y = 0.1492 * x^\wedge(-1.094) + 1.395$	0.4195	0.9998
	15	8~65	$y = 0.07014 * x^\wedge(-1.187) + 2.264$	0.6893	0.9994
	20	8~65	$y = 0.04705 * x^\wedge(-1.207) + 2.135$	0.5677	0.9992
	25	8~65	$y = 0.04128 * x^\wedge(-1.188) + 1.816$	0.5110	0.9990

[a] RMSE: root mean squared error

[b] R-square: coefficient of determination, which reflects the fitting accuracy

0.9 and 1.0. The influence of D on the CFSCs for $\beta = 45°$ and $m_i = 10$ is shown in Fig. 4, from which it can be found that the CFCSs rise with the increase of D. The ratio of the CFSCs ($D \neq 0$) to the CFSCs ($D = 0$) remains almost constant when s^α varies, which can be represented by the equation below.

$$
\begin{aligned}
R_D(D \neq 0) &= \left. \frac{\sigma_{ci}/\gamma H \, (D \neq 0)}{\sigma_{ci}/\gamma H \, (D = 0)} \right|_{s^\alpha} \\
&= \frac{\sigma_{ci}/\gamma H \cdot s^\alpha (D \neq 0)}{\sigma_{ci}/\gamma H \cdot s^\alpha (D = 0)} \\
&= \frac{\lambda(D \neq 0)}{\lambda(D = 0)}.
\end{aligned} \tag{17}
$$

Therefore, the CFSCs of $D \neq 0$ can be obtained by multiplying the CFSCs of $D = 0$ by the ratio R_D. The estimation of the ratio R_D for different β and m_i can be solved by simulation analysis. The procedure is as follows: for $\beta = 45°$, mi is set to 5, 10, 15, 20 and 25. The parameters at the critical failure state for $D = 0$, 0.5, 0.7, 0.9 and 1.0 are searched for the given s^α, and the dimensionless parameter λ and the ratio R_D for 0.5, 0.7, 0.9 and 1.0 are calculated with Eq. (17). Figure 5 shows that the dimensionless parameter λ varies with m_i for different D at $\beta = 45°$, 60° and 75°. Figure 6 shows that the ratio R_D for $D = 0.5$, 0.7, 0.9, and 1.0 varies m_i at $\beta = 45°$, 60° and 75°. With the ratio R_D and the CFSCs for $D = 0$ obtained from "Explicit expression of the CFSC by numerical simulation", the CFSCs of $D = 0.5$, 0.7, 0.9, and 1.0 for different mi and β can be obtained.

SRM based on the slope CFSC

Reduction strategy for the GHB criterion

With the theoretical existence of CFSC proved and the explicit expression of CFSC obtained, a new reduction strategy based on the compressive strength of rock mass for the GHB criterion was proposed, which can better reflect the physical meaning of strength reduction than the direct reduction of material parameters. In this strategy, the compressive strength of intact rock σ_{ci} and the parameter combination s^α are reduced by the same ratio, where s^α is numerically equivalent to Jointing Parameter (JP) of Palmström's RMi system (Russo 2008), which represented the rock mass quality and structure. m_i, as a parameter representing the degree of intact rock hardness, should not be involved in reduction. However, with the decrease in GSI, the parameter of rock mass m_b will decrease correspondingly. According to the GHB criterion of the 2018 edition (Hoek and Brown 2019), the compressive to tensile ratio and the parameter m_i satisfy the approximate relationship in Eq. (18). Thus, the same reduction ratio of the compressive strength and the tensile strength of intact rock can be realized by keeping m_i constant.

$$
\sigma_{ci}/|\sigma_t| = 0.81 m_i + 7. \tag{18}
$$

The disturbance factor D, which is subjected to blast damage and stress relaxation, should not participate in the reduction. The reduction of s^α is only determined by the
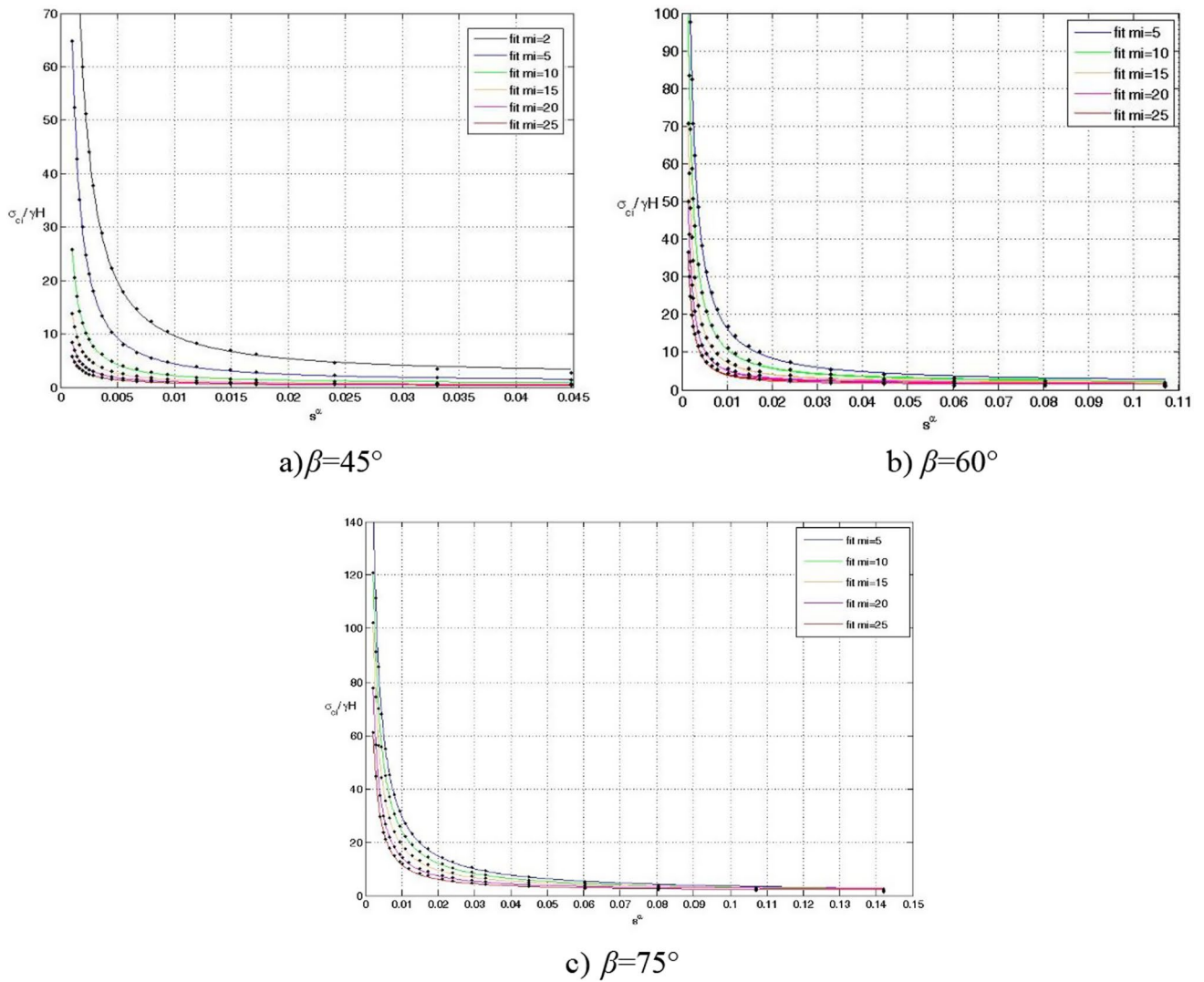
a) $\beta=45°$

b) $\beta=60°$

c) $\beta=75°$

Fig. 3 The fitting curves of CFSCs for different m_i and β *values*

a) The CFSCs with different values of D

b) The ratio R_D *varies with* s^α
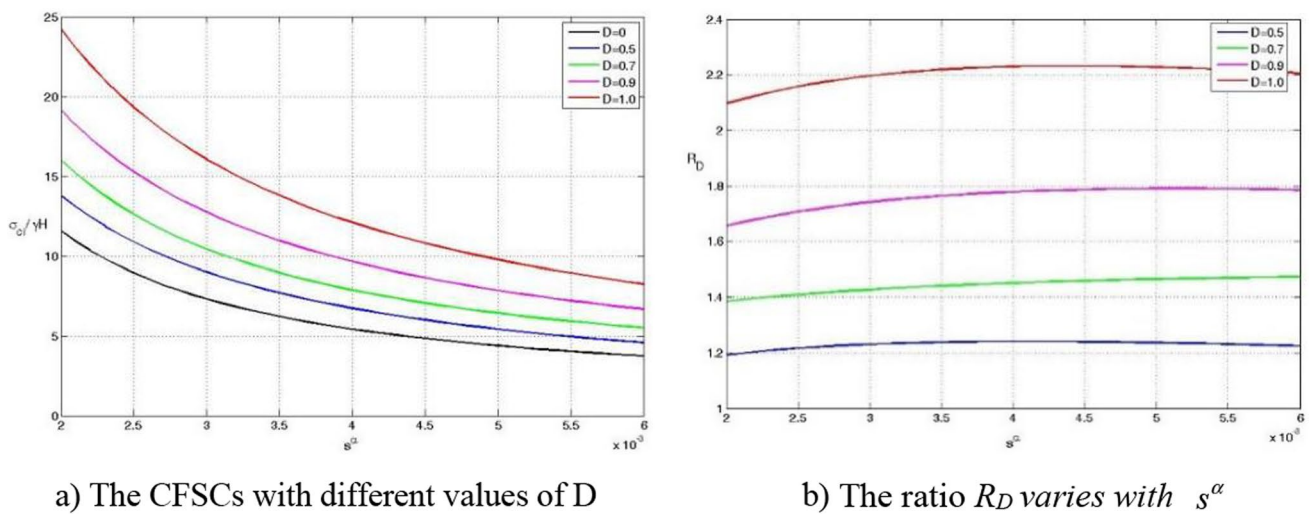
Fig. 4 The CFSCs with different values of D and the ratio R_D *varies with* s^α for $\beta=45°$ and $m_i=10$
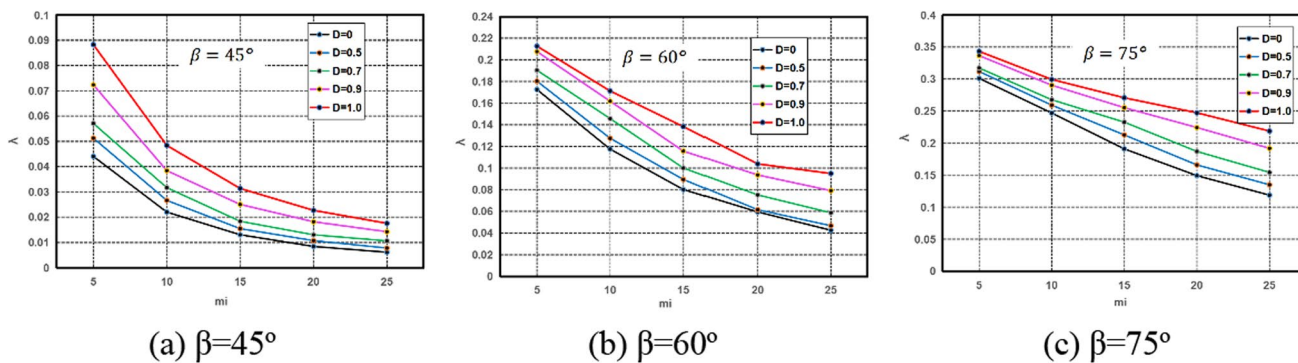
Fig. 5 The dimensionless parameter λ varies with m_i for different D at $\beta = 45°$, $60°$ and $75°$
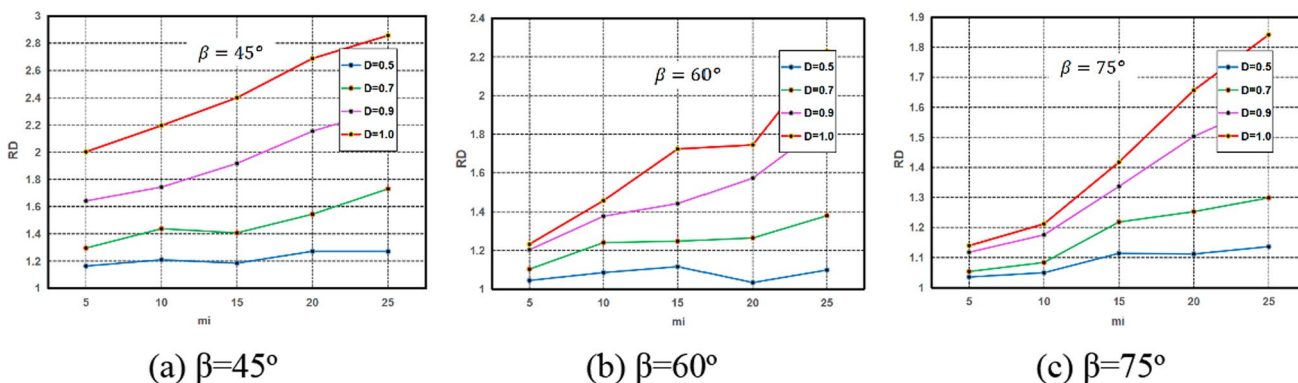

Fig. 6 The ratio R_D for $D = 0.5$, 0.7, 0.9, and 1.0 varies with m_i at $\beta = 45°$, $60°$ and $75°$

reduced *GSI*. The reduction strategy can be expressed by the formula in Eq. (19).

$$K_r = \frac{\sigma_{ci}^t}{\sigma_{ci}^r} = \frac{s^{t\,\alpha^t}}{s^{r\,\alpha^r}} = \frac{f(GSI^t)}{f(GSI^r)}, \tag{19}$$

where K_r is the reduction ratio and σ_{ci}^t, s^t and α^t are the parameters of the target slope. σ_{ci}^r, s^r and α^r are the parameters of the reduced slope.

According to the CFSC, the reduction strategy can be replaced by reducing the parameter $\sigma_{ci}/\gamma H$ and the parameter combination s^α by the same ratio represented by the formula in Eq. (20), because γH is constant during the reduction procedure.

$$K_r = \frac{\sigma_{ci}^t / \gamma H}{\sigma_{ci}^r / \gamma H} = \frac{s^{t\,\alpha^t}}{s^{r\,\alpha^r}}. \tag{20}$$

The reduction scheme relative to CFSC can be represented by Fig. 7a, in which the reduction ratios for $\sigma_{ci}/\gamma H$ and s^α are the same.

According to the reduction strategy, when the slope CFSC fitting formula is determined, the slope critical state parameters can be directly determined by mathematical calculation (the point of intersection of the CFSC and the proportional line determined by the target point) without the need for simulation analysis. The parameters (GIS^r and σ_{ci}^r) at the critical failure state are determined by the critical state points ($s^{r\,\alpha^r}$ and $\sigma_{ci}^r / \lambda H$). The reduction scheme was applied to several slope examples to determine the value of critical state parameters by the MATLAB program. The graph of the example for $\beta = 60°$ and $m_i = 5$ by applying this strategy is displayed in Fig. 7b.

To verify the feasibility of this scheme, 15 slope examples with different slope angles β, m_i values and other parameters of initial states (shown in Table 3) were applied by this reduction strategy to predict the critical state parameters. The disturbance coefficient D was assigned to 0 to simplify the procedure. The model numerical analysis was realized by establishing the numerical slope model and continuously reduce the strength parameters by the reduction rule in Eq. (20) until the strength parameters of the critical state are obtained. The parameters predicted by this strategy were compared with those obtained by simulation model analysis. The results are shown in Table 3.
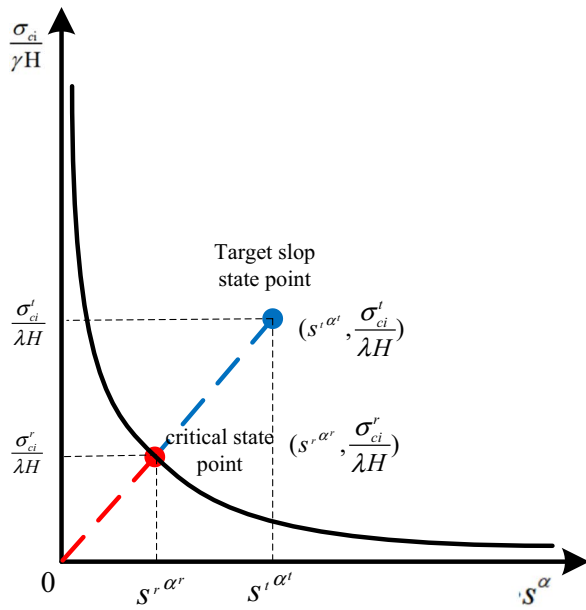
(a) The graphic representation of the reduction strategy
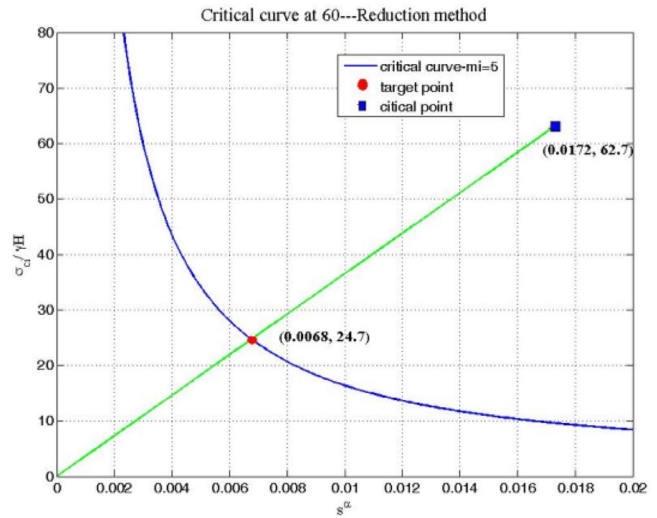
(b) The slope example for m_i=5, β=60°

Fig. 7 The graphic representation of the reduction strategy and the example for $m_i=5$, $\beta=60°$

Table 3 The comparison results of the predicted parameters and simulation parameters for the critical state

Angle β Height H (m)	Value of m_i	Parameters of the initial state (σ_{ci}: MPa)	Parameters of the critical state determined by CFSC (σ_{ci}: MPa)	Parameters of the critical state by simulation analysis (σ_{ci}: MPa)	The absolute error of λ	The relative error of λ
$\beta=45°$ $H=50$	$m_i = 5$	$GSI = 25, \sigma_{ci} = 30$	$GSI = 14.6, \sigma_{ci} = 12.15\lambda = 0.0457$	$GSI = 14.6, \sigma_{ci} = 12.2\lambda = 0.0459$	-0.0002	-0.4%
	$m_i = 10$	$GSI = 25, \sigma_{ci} = 40$	$GSI = 10.1, \sigma_{ci} = 9.55\lambda = 0.0218$	$GSI = 10.1, \sigma_{ci} = 9.8\lambda = 0.0223$	-0.0006	-2.6%
	$m_i = 15$	$GSI = 20, \sigma_{ci} = 40$	$GSI = 6.5, \sigma_{ci} = 9.35\lambda = 0.01327$	$GSI = 6.5, \sigma_{ci} = 9.3\lambda = 0.01320$	$7.1E-05$	0.5%
	$m_i = 20$	$GSI = 20, \sigma_{ci} = 30$	$GSI = 6.1, \sigma_{ci} = 6.24$ $\lambda = 0.00836$	$GSI = 6.1, \sigma_{ci} = 6.2$ $\lambda = 0.00831$	$5.4E-05$	0.6%
	$m_i = 25$	$GSI = 15, \sigma_{ci} = 30$	$GSI = 3.3, \sigma_{ci} = 6.7$ $\lambda = 0.00581$	$GSI = 3.3, \sigma_{ci} = 6.7$ $\lambda = 0.00590$	$8.7E-05$	-1.5%
$\beta=60°$ $H=51$	$m_i = 5$	$GSI = 30, \sigma_{ci} = 80$	$GSI = 18.1, \sigma_{ci} = 31.7$ $\lambda = 0.1672$	$GSI = 18.1, \sigma_{ci} = 31.2$ $\lambda = 0.1646$	0.0026	1.6%
	$m_i = 10$	$GSI = 40, \sigma_{ci} = 60$	$GSI = 21.1, \sigma_{ci} = 15.9$ $\lambda = 0.1090$	$GSI = 21.1, \sigma_{ci} = 16.2$ $\lambda = 0.1111$	-0.0021	-1.8%
	$m_i = 15$	$GSI = 30, \sigma_{ci} = 30$	$GSI = 19.1, \sigma_{ci} = 12.8$ $\lambda = 0.0739$	$GSI = 19.1, \sigma_{ci} = 13.1$ $\lambda = 0.0756$	-0.0017	-2.3%
	$m_i = 20$	$GSI = 30, \sigma_{ci} = 30$	$GSI = 17.8, \sigma_{ci} = 10.7$ $\lambda = 0.0549$	$GSI = 17.8, \sigma_{ci} = 10.5$ $\lambda = 0.0539$	0.0010	1.9%
	$m_i = 25$	$GSI = 30, \sigma_{ci} = 30$	$GSI = 15.8, \sigma_{ci} = 9.4$ $\lambda = 0.0399$	$GSI = 15.8, \sigma_{ci} = 9.6$ $\lambda = 0.0407$	-0.0008	-2.1%
$\beta=75°$ $H=37$	$mi = 5$	$GSI = 40, \sigma_{ci} = 40$	$GSI = 28.8, \sigma_{ci} = 18.2$ $\lambda = 0.2162$	$GSI = 28.8, \sigma_{ci} = 18.2$ $\lambda = 0.2197$	-0.0036	-1.6%
	$mi = 10$	$GSI = 35, \sigma_{ci} = 60$	$GSI = 22.1, \sigma_{ci} = 23.8\lambda = 0.1773$	$GSI = 22.1, \sigma_{ci} = 23.8\lambda = 0.1773$	0.0000	0%
	$mi = 15$	$GSI = 30, \sigma_{ci} = 50$	$GSI = 19.8, \sigma_{ci} = 22.7$ $\lambda = 0.1393$	$GSI = 19.8, \sigma_{ci} = 22.8\lambda = 0.1399$	-0.0006	-0.4%
	$mi = 20$	$GSI = 40, \sigma_{ci} = 30$	$GSI = 25.4, \sigma_{ci} = 11.2\lambda = 0.1082$	$GSI = 25.4, \sigma_{ci} = 11.4\lambda = 0.1101$	-0.0019	-1.8%
	$mi = 25$	$GSI = 30, \sigma_{ci} = 60$	$GSI = 16.2, \sigma_{ci} = 19.7\lambda = 0.0869$	$GSI = 16.2, \sigma_{ci} = 19.7\lambda = 0.0860$	0.0009	1.0%

From the results of Table 3, it can be seen that the relative errors between the parameters of the critical state predicted by the CFSC and the parameters obtained by simulation analysis are lower than 3%, which proves the validity and accuracy of this strategy.

The analysis of the influence of m_i reduction

To determine whether m_i should be reduced, three slope examples given in this paper are reduced and analysed by applying the strength reduction above. The parameters of the three slope examples are shown in Table 4. The parameters at the slope critical failure state are obtained by numerical simulation with the decrease in m_i from the initial value. With the critical state parameters, the curves of shear stress to the normal stress of the slope are drawn to analyse the influence of m_i decreasing on the strength envelope of the GHB criterion.

The curves of shear stress to the normal stress of the three slopes at the initial state and the critical failure state are shown in Fig. 8a. It can be seen that the strength envelopes are very close with decreasing mi. The shear stress ratio of the initial state to the critical state varies with the normal stress which is shown in Fig. 8b. When the value of mi decreases by Ratio$_{mi}$ = 1 ~ 1.5 (Eq. 21), the shear stress ratio increases less than 0.12, which means the reduction of m_i has little inference to the shear strength. According to the conservative principle, the strength envelope is the highest and the shear stress ratio is the smallest when m_i is not reduced, corresponding to the lowest safety factor.

$$\text{Ratio}_{mi} = m_{i\text{ - initial}} \big/ m_{i\text{ - reduced}}. \tag{21}$$

The definition of factor of safety

The definition of a factor of safety (FOS) is the key to slope stability evaluation. In rock slope engineering, the safety factor is often defined by the ratio of anti-sliding force and sliding force on the sliding surface of the slope. This method relies heavily on the determination of the sliding surface, for example, the global safety factor defined by Yuan et al. (2020). Some scholars directly used the reduction ratio of the GHB criterion parameters as the

safety factor to simplify the analysis procedure, which is obviously unreasonable. According to the strength reduction strategy in "Reduction strategy for the GHB criterion", the strength parameters of the initial state and critical state have been obtained, based on which, a new factor of safety (FOS) definition method independent of sliding surface determination was proposed. In this method, the ratio of the average shear strength between the target state and the critical state was taken as the FOS of the slope, where the average shear strength at the critical failure state represents the sliding force per unit area, and the average shear strength at the initial state represents the sliding resistance force per unit area, which satisfies the meaning of strength reserve. The average shear strength with the range of the normal stress shows overall mechanical behaviour.

The specific calculation process is as follows:

(1) The range of minimum principal stress σ_3 at the critical state is determined by Eq. (22) based on the literature (Hoek et al. 2002)

$$\begin{cases} \sigma_{3\max} = 0.72\sigma_{cm}\left(\dfrac{\sigma_{cm}}{\gamma H}\right)^{-0.91} \\ \sigma_{cm} = \sigma_{ci} \cdot \dfrac{(m_b + 4s - \alpha(m_b - 8s))(m_b\big/4 + s)^{\alpha-1}}{2(1+\alpha)(2+\alpha)} \end{cases}, \tag{22}$$

where σ_{cm} represents the global "rock mass strength" reflecting the overall behaviour of a rock mass. $\sigma_{3\max}$ is the upper limit of the minimum principal stress for slopes. σ_{ci}, m_b, s, and α are the parameters at the critical state.

(2) The normal stress σ_n and the shear stress τ at the initial state and the critical state, respectively, are calculated with the corresponding parameters by Eq. (5), and the upper limit of σ_n at the initial state and the critical state ($\sigma_{n\max}^t$ and $\sigma_{n\max}^r$) were calculated with the upper limit $\sigma_{3\max}$ at the critical state.

(3) The arithmetic mean value of shear stress τ within the range σ_n obtained by step 2 is taken as the average shear strength, and the ratio of the average shear strength of the target state to the critical state is taken as the FOS. The formula is as follows:

Table 4 The geometry and material parameters of the three slope examples

Parameters	H /m	β	γ/ kN/m³	σ_{ci} /MPa	GSI	m_i	D	m_b	s	α
Slope 1	20	45°	25	30	10	10	0	0.067	$2.5* 10^{-5}$	0.619
Slope 2	34	60°	25	50	30	15	0	0.171	$3.9* 10^{-5}$	0.523
Slope 3	37	75°	25	80	40	25	0	0.281	$1.6* 10^{-4}$	0.508
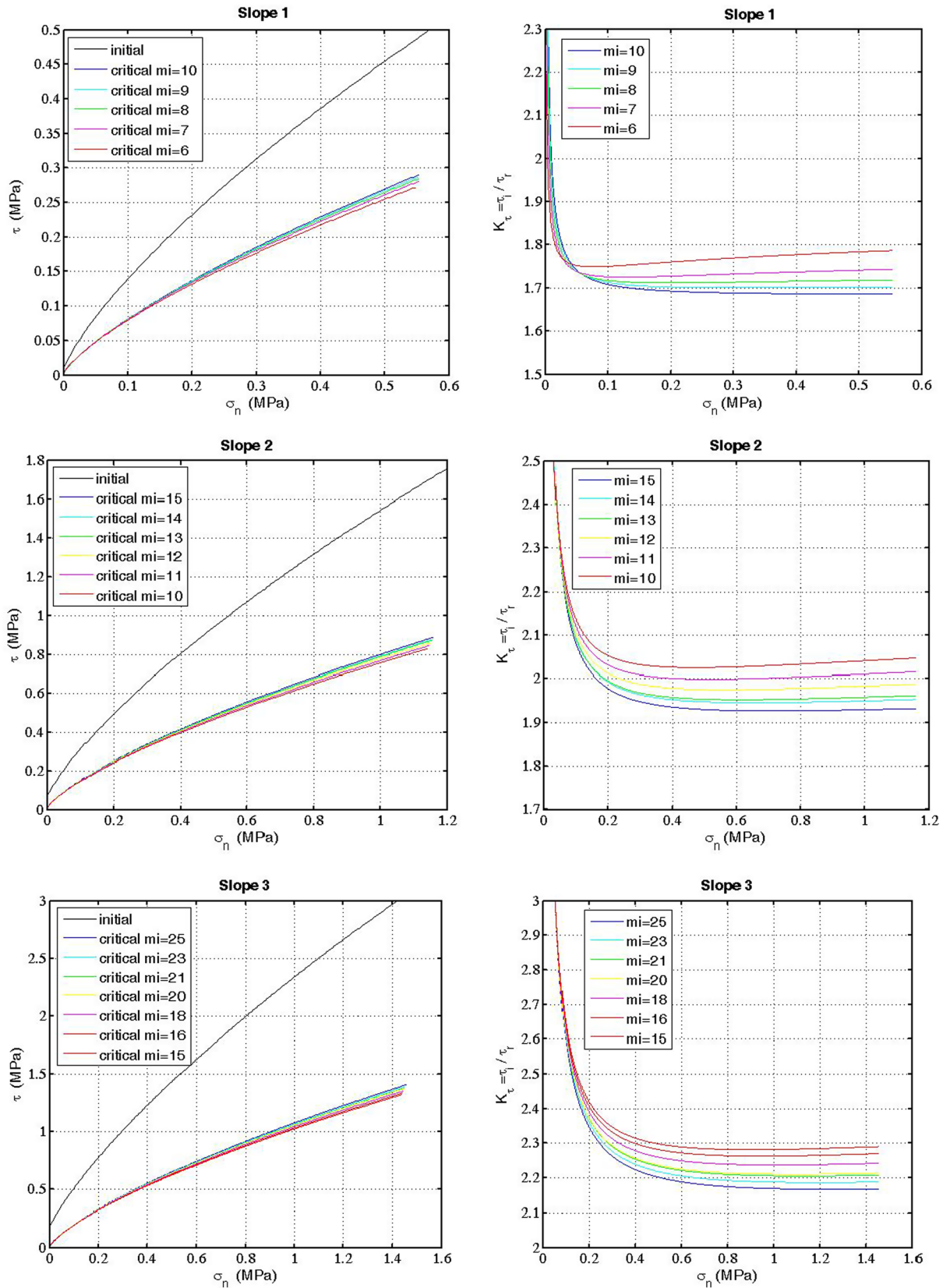
a) The shear stress to normal stress   b) The shear stress ratio of the initial state to the critical state

Fig. 8 The curves of shear stress and the shear stress ratio of the three slopes

$$F_s = \frac{\overline{\tau^t}}{\overline{\tau^r}} = \frac{\int_0^{\sigma_{n\max}^t} \tau^t d\sigma_n / \sigma_{n\max}^t}{\int_0^{\sigma_{n\max}^r} \tau^r d\sigma_n / \sigma_{n\max}^r}. \tag{23}$$

The analysis of slope examples

To verify the validity and accuracy of the proposed method in slope stability analysis, several slope examples selected from the published literature were analysed and discussed. These slope examples are the classical examples that have been repeatedly used in the literature of SRM based on GHB criterion and some of them are from practical engineering cases (Example 9). The examples were classified into two groups for $D=0$ and $D\neq0$. The slope parameters at the initial state are shown in Tables 5 and 6. First, the parameters at the critical failure state obtained by the graphic method based on CFSCs were compared with those obtained by

Table 5 The slope geometry and rock mass parameters at the initial state for $D=0$

Example	Height H (m)	Angle β	E (MPa)	ν	γ (kN/m³)	σ_{ci} (MPa)	GSI	m_i	D	mb	s	α
1 Hammah et al. (2005)	10	45°	5000	0.3	25	30	5	2	0	0.067	$2.6*10^{-5}$	0.619
2 Sukany et al. (2012)	10	45°	5000	0.3	25	15	5	7	0	0.235	$2.6*10^{-5}$	0.619
3 Shen et al. (2013)	50	45°	5000	0.3	27	13.5	30	5	0	0.410	$4.2*10^{-4}$	0.522
4 Shen et al. (2013)	25	60°	5000	0.3	23	20	30	8	0	0.657	$4.2*10^{-4}$	0.522

Table 6 The slope geometry and rock mass parameters at the initial state for $D\neq0$

Example	Height H (m)	Angle β	E (MPa)	ν	γ (kN/m³)	σ_{ci} (MPa)	GSI	m_i	D	mb	s	α
5 Shen et al. (2013)	50	45°	5000	0.3	27	13.5	30	5	0.7	0.107	$3.93*10^{-5}$	0.522
6 Shen et al. (2013)	25	45°	5000	0.3	27	5.4	20	20	0.7	0.247	$9.22*10^{-6}$	0.544
7 Sun et al. (2016)	80	60°	5000	0.3	21	40	37	9	1.0	0.100	$2.75*10^{-5}$	0.514
8 Thomas et al. (2008)	32	75	5000	0.3	25	40	45	10	0.9	0.281	$1.6*10^{-4}$	0.508
9 Sari (2019)	25	75	64,350	0.25	27	184	63	10.7	0.7	1.396	$4.7*10^{-3}$	0.502

Note: a.relative error$_\lambda = \frac{\lambda_{graphic}-\lambda_{simulation}}{\lambda_{simulation}} \times 100\%$

Table 7 The slope rock mass parameters at the critical failure state for $D=0$

Example	Simulation analysis						Graphically analysis						Relative error of λ[a]
	σ_{ci} (MPa)	GSI	m_b	s	α	λ	σ_{ci} (MPa)	GSI	m_b	s	α	λ	
1	26.0	4	0.065	$2.33*10^{-5}$	0.627	0.1290	25.8	4.05	0.065	$2.34*10^{-5}$	0.627	0.1290	0%
2	10.9	3	0.219	$2.08*10^{-5}$	0.636	0.0458	10.7	2.95	0.219	$2.07*10^{-5}$	0.637	0.0446	−2.7%
3	6.9	21	0.298	$1.54*10^{-4}$	0.541	0.0443	6.82	21	0.298	$1.54*10^{-4}$	0.541	0.0438	−1.2%
4	8.5	19	0.443	$1.23*10^{-4}$	0.546	0.1078	8.8	19.5	0.451	$1.30*10^{-4}$	0.545	0.1110	8.0%

Table 8 The slope rock mass parameters at the critical failure state for $D\neq0$

Example	Simulation analysis						Graphically analysis						Relative error of λ
	σ_{ci} (MPa)	GSI	mb	s	α	λ	σ_{ci} (MPa)	GSI	mb	s	α	λ	
5	14.4	30.7	0.111	$4.35*10^{-5}$	0.521	0.0568	14.7	30.9	0.112	$4.47*10^{-5}$	0.521	0.0590	3.9%
6	4.80	19.0	0.233	$7.98*10^{-6}$	0.547	0.0116	5.0	19.5	0.240	$8.57*10^{-6}$	0.545	0.0128	10%
7	51.6	39.8	0.122	$4.39*10^{-5}$	0.512	0.181	50.6	39.5	0.120	$4.18*10^{-5}$	0.512	0.173	−4.4%
8	26.8	40.4	0.209	$7.79*10^{-5}$	0.511	0.266	26.4	40.2	0.206	$7.54*10^{-5}$	0.511	0.258	3.0%
9	21.1	35	0.301	$8.11*10^{-5}$	0516	0.0672	20.6	34.7	0.296	$7.76*10^{-5}$	0.516	0.0638	−5.1%

Table 9 The comparison of FOS of slope examples by different methods

Example		main parameters				FOS				Relative error of FOS [a]			Stability state
		H	β	m_i	D	Graphic method	Simulation analysis	Bishop simplified	Local linearization	Simulation analysis	Bishop simplified	Local linearization	
D=0	1	10	45°	2	0	1.162	1.164	1.172	1.160	−0.17%	−0.86%	0.17%	Basically stable
	2	10	45°	7	0	1.278	1.290	1.355	1.324	−0.94%	−6.03%	−3.60%	Stable
	3	50	45°	5	0	1.646	1.637	1.600	1.574	0.55%	2.87%	4.57%	Stable
	4	25	60°	8	0	1.834	1.887	2.122	1.84	−2.81%	−13.57%	−0.33%	Stable
D≠0	5	50	45°	5	0.7	0.932	0.947	0.984	0.963	−1.61%	−5.58%	−3.33%	Unstable
	6	25	45°	20	0.7	1.057	1.092	1.094	1.082	−3.31%	−3.50%	−2.37%	Metastable
	7	80	60°	9	1.0	0.815	0.798	0.986	0.78	2.09%	−17.34%	4.29%	Unstable
	8	32	75°	10	0.9	1.420	1.400	1.457	1.38	1.41%	−2.61%	2.82%	Stable
	9	25	75°	10.7	0.7	13.02	12.72	12.411	12.68	2.30%	4.68%	2.61%	Stable

Note: a. relative error$_{FOS} = \frac{FOS_{graphic\text{-}method} - FOS_{other\text{-}method}}{FOS_{other\text{-}method}} \times 100\%$

numerical simulation, of which the results are shown in Tables 7 and 8. From the table, it can be seen that the relative error of dimensionless parameter λ is less than 8% for $D=0$ and less than 10% for $D \neq 0$. This proves that the CFSCs for $D=0$ and mi $\neq$ 5,10,15,20,25 obtained by cubic spline interpolation have high accuracy, and the CFSCs for $D \neq 0$ obtained by the D ratio are relatively accurate.

According to the definition of the factor of safety in "The definition of factor of safety", the FOS of these slope examples can be calculated with the initial and critical parameters. To verify the validity and accuracy of the reduction strategy and the definition of FOS, the results obtained by graphic analysis and simulation analysis were compared with the FOS obtained by the local linearization method and the Bishop simplified (limit equilibrium method). The results are shown in Table 9.

The local linearization method (LLM), as a sophisticated SRM, has been applied in FLAC^{3D} for solving the FOS of the HB criterion slope. This method is physically more correct than the global approach (Sukanya et al. 2012). Among the Limit equilibrium method (LEM), the Bishop simplified method is a well-known technique and widely applied in slope stability analysis of civil engineering. The LEM is limited by the concepts of circular sliding surfaces and slice, while SRM based on finite element analysis can directly obtain the sliding surface of the slope by considering the stress–strain relationship without the shape assumption of the sliding surface, which made SRM more accuracy and reasonable than LEM (Zhao et al. 2002, 2005). The model analysis and the calculation of FOS with LLM were based on the software FLAC^{3D} 6.0. The model analysis of the FOSs obtained with Bishop's simplified method were achieved based on the software Slide 6.0.

The FOS obtained by the proposed method (graphic method) is very close to that of the simulation analysis with the same FOS definition (relative error $< \pm 5\%$). Moreover, the error between the proposed method and the local linearization method is also very low (relative error $< \pm 5\%$). The results of the proposed method are usually smaller than that of the Bishop simplified method, with a relative error lower than 20%.

Discussion

The FOSs obtained by the proposed method are very close to the results of the LLM with an absolute relative error smaller than 5%, has an acceptable error compared with the Bishop simplified method. Moreover, the relative error decreases as the FOS approaches 1.0. According to the literature (Du SG 2018), the slope stability state can be classified by FOS in Table 10. By comparing the FOS, it can be found that the proposed method has the same stability state as the other

Table 10 The relationship between the FOS and stability state

Stability level	Level 1	Level 2	Level 3	Level 4
FOS	0–1.05	1.05–1.15	1.15–1.25	> 1.25
Stability State	Unstable	Metastable	Basically stable	Stable

two methods. The calculation speed and efficiency of the proposed method have a large improvement compared with simulation analysis and local linearization method, where searching for an appropriate reduction ratio takes considerable calculation time.

The analysis of engineering case

The proposed SRM-based GHB criterion was applied to a limestone slope of an open pit mine located at the junction of central Hebei Plain and Taihang Mountain, in Luquan District, Shijiazhuang City, Hebei province, China. The main mineral components of the ore layer are calcite, dolomite and a small amount of clay minerals. The ore layer is thickly layered, with block and porphyritic structure, weak weathering and relatively intact. The mining area is 0.7972 km^2, and the end slope forms 6 steps (the length for each step is 70 ~ 280 m, the step height is 15 m, the step width is 8-12 m, and the step slope angle is about $65^\circ \sim 75^\circ$). The final slope height is about 90 m with a 50° slope angle, and the 3D point cloud map is shown in Fig. 9a. To simplify the analysis procedure, a typical section was chosen to establish the slope model, shown in Fig. 9b. Based on geological observations and laboratory experiments, the material parameters of rock mass are obtained and shown

below: $\gamma = 27$ kN/m^3, $m_i = 8$, $\sigma_{ci} = 40$ MPa, $GSI = 45$, $D = 0.9$, $E = 50$GPa.

Although the limestone slope has multiple steps, an equivalent single-step slope based on the final slope height and slope angle (H = 90 m, $\beta = 50^\circ$) can be applied for the proposed graphical method. The detailed analysis procedure was below:

(1) The fitting expressions of the CFSCs for $m_i = 8$, $\beta = 45^\circ$, $D = 0$ and $m_i = 8$, $\beta = 60^\circ$, $D = 0$ were deduced by the cubic spline interpolation based on the fitting expressions in Table 2. The expressions of the CFSCs for $m_i = 8$, $\beta = 50^\circ$, $D = 0$ was obtained by linear interpolation of two corresponding CFSCs at $\beta = 45^\circ$ and $\beta = 60^\circ$.

(2) The fitting expressions of the CFSCs for $m_i = 8$, $\beta = 50^\circ$, $D = 0.9$ are deduced by multiplying the CFSC of $m_i = 8$, $\beta = 50^\circ$, $D = 0$ with the corresponding ratio R_D obtained from "The influence of disturbance factor D on the CFSCs", and the explicit expression of the CFSCs for $m_i = 8$, $\beta = 50^\circ$, $D = 0.9$ was shown in Eq. (24).

$$y = 0.01496 * \wedge(-1.279) + 1.609. \tag{24}$$

(3) The parameters of the critical failure state are obtained from the initial state parameters by reducing σ_{ci} and s^α with the same ratio defined in Eq. (20), and the graphical analysis was shown in Fig. 10, where the red curve represents the CFSC for $m_i = 8$, $\beta = 50^\circ$, $D = 0.9$, the green line represents the reduction path, and the intersection point was determined by the critical state parameters, which can be deduced by the reduction strategy in Eq. (25). The critical state parameters are calculated, ($\sigma_{ci}^r = 22.8MPa, GSI^r = 38.5$), shown in Table 11.
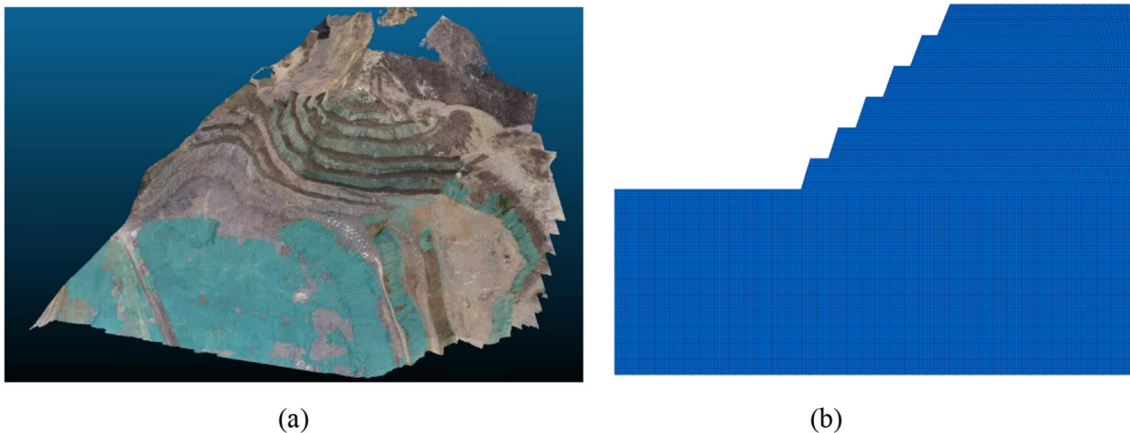

(a)   (b)

Fig. 9 The 3D point cloud map and its typical section of the open pit slope

$$\begin{cases} \sigma_{ci}^r / \gamma H = 10.55 \\ s^{r \, \alpha^r} \big|_{D=0.9} = \exp\left(\left(\frac{GSI^r - 100}{9 - 3D}\right)\left(\frac{1}{2} + \frac{1}{6}(e^{-\frac{GSI^r}{15}} - e^{-\frac{20}{3}})\right)\right)\Big|_{D=0.9} = 0.0067 \end{cases} \tag{25}$$

(4)　The FOS of the slope was calculated by the definition of Eq. (24) based on the parameters f the initial and critical states, and the results was shown in Table 12.

　The slope model based on the typical section is established in FLAC³ᴰ and the parameters of the critical failure state were obtained by constantly reduce the parameters σ_{ci} and GSI with the same reduction strategy defined in Eq. (20) until the slope reaches the critical failure state, shown in Table 11. The numerical simulation analysis and the maximum shear strain increment contour at the critical

failure state is shown Fig. 11a. The numerical analysis based on the local linearization method and the result is shown Fig. 11b. The analysis result of the Bishop simplified method based on the software Slide was shown in Fig. 12.

　The FOSs obtained by different methods were shown in Table 12. The results show that the FOS obtained by the proposed graphical analysis method is between that of the Bishop simplified and simulation analysis. Compared with other methods, the *FOS* relative error of the Graphical analysis method is less than 10%, and the stability state for different methods are perfectly the same. The results

Fig. 10 The demonstration of the graphical method of the slope case
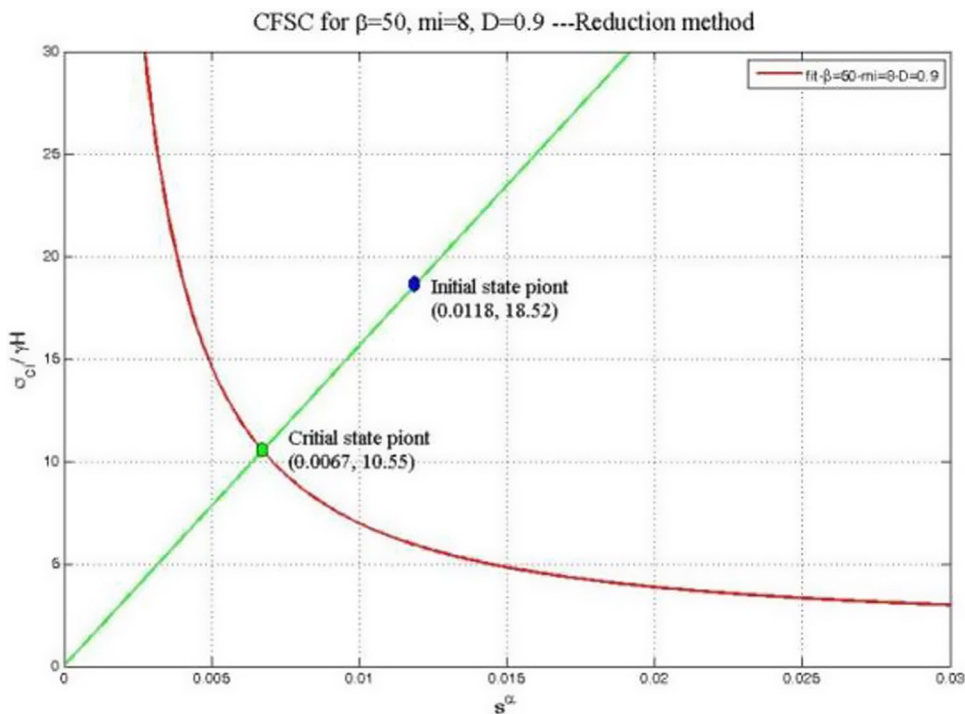

Table 11 The parameters of the slope case at initial state and critical failure state

Parameters	H (m)	β	γ (kN/m³)	mi	D	σ_ci (MPa)	GSI	mb	s	α	λ
Initial state	90	50°	27	8	0.9	40	45	0.281	$1.62*10^{-4}$	0.508	0.1950
Critical state (simulation analysis)						21.7	38	0.178	$5.32*10^{-5}$	0.513	0.0572
Critical state (graphical analysis)						22.8	38.5	0.184	$5.76*10^{-5}$	0.513	00626

Table 12 The FOSs obtained by different methods and expert analysis report

Methods	Graphical analysis	Simulation analysis	Bishop simplified Method	Local linearization Method
FOS	1.618	1.684	1.573	1.510
Relative error $_{FOS}$	–	−3.92%	2.86%	7.15%
Stability State	Stable	Stable	Stable	Stable

demonstrate the feasibility and validity of the proposed graphical method in the practical engineering slope case with complex slope form. Moreover, the proposed graphical analysis method demonstrates its great advantages in computation amount and time without the model establishment and the multiple numerical analysis of stability.

Conclusions

This paper proposed a new SRM (graphic method) based on the CFSCs. First, the CFSCs are established based on a large amount of simulation data, the influence of m_i and D on the CFSCs are analysed, and the explicit expressions

(a) Numerical simulation analysis   （b) Local linearization method
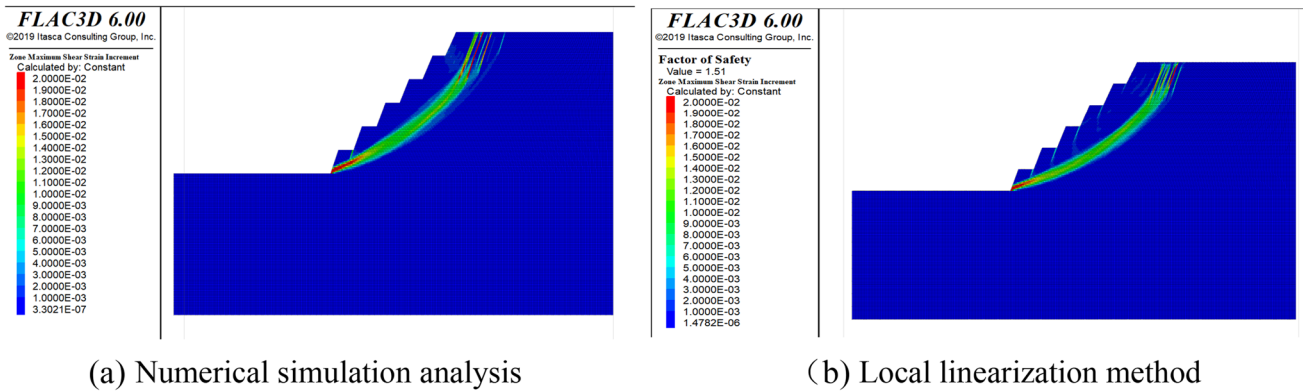
Fig. 11 The maximum shear strain contour at the critical failure state with numerical simulation analysis and local linearization method

Fig. 12 The results of Bishop's simplified method with Slide software
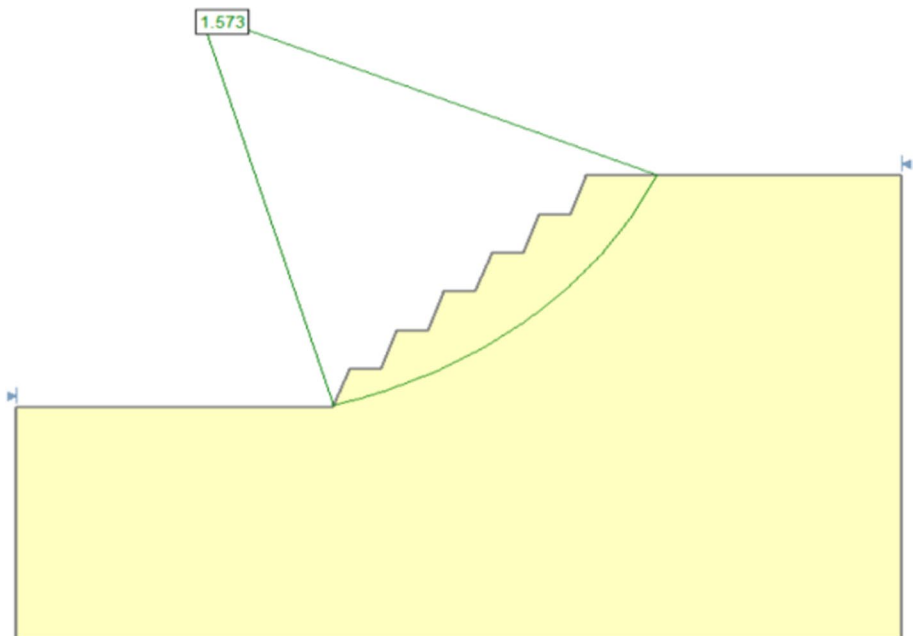
of the CFSCs are determined by curve fitting. Then, the new strength reduction scheme with the same reduction ratio for σ_{ci} and s^α based on the CFSCs, and the new definition method of FOS was proposed. This new method was applied to nine slope examples and a practical case of an open pit slope to verify its validity and accuracy. The main conclusions are as follows:

(1) The parameters $\left(\frac{\sigma_{ci}}{\gamma H}, s^\alpha, mi, \beta\right)$ satisfy a relationship at the critical failure state by theoretical analysis. For given m_i and β, the relation between $\frac{\sigma_{ci}}{\gamma H}$ and s^α can be represented by an exponential function. These curves are called CFSCs.

(2) The variations of the CFSCs with m_i and D are analysed. The CFSCs for any value of m_i can be obtained by cubic spline interpolation. The CFSCs for $D \neq 0$ can be obtained by multiplying the CFSCs of $D = 0$ by the ratio R_D.

(3) A new reduction strategy based on CFSCs is proposed, where σ_{ci} and s^α are reduced by the same ratio, m_i remains constant to guarantee the same reduction ratio of the compressive strength and the tensile strength of intact rock, and D subjected to blast damage and stress relaxation should not be reduced. The reduction in σ_{ci} and s^α, representing the strength of intact rock and joint parameters (JP) of the rock mass, respectively, can better reflect the strength reduction of the rock mass. The parameters at the critical state can be obtained by the graphic method based on the CFSCs.

(4) By comparing the critical state parameters obtained by the graphic method and that from the simulation analysis of slope examples, the CFSCs for different m_i and D have a high accuracy.

(5) A new definition method of FOS, independent of sliding surface, based on the parameters of the initial and critical states, was proposed. By the analysis of nine slope examples, the results showed that FOSs obtained by the graphic reduction method and the new definition of FOS are close to the results of the local linearization method (LLM) and the Bishop simplified method, with $\pm 5\%$ relative error compared with the LLM. The accuracy of FOS increases when FOS approaches 1.0, and the stability state assessments by the proposed method are perfectly accurate. The results comparison verified the validity and reliability of the SRM and the FOS definition proposed. The proposed method was applied to a practical case of an open pit limestone slope with multiple steps to demonstrate its feasibility and reliability in engineering application.

(6) The calculation speed and efficiency of the graphic method have a significant improvement compared with the simulation analysis and the LLM, where searching for an appropriate reduction ratio and multiple numerical analysis of stability take considerable calculation time. Under the same computational power, the proposed method based on computation of MATLAB software need less than 30s to search the critical state parameters and calculate the safety factor, while the simulation analysis based on model equilibrium computation of FLAC^{3D} software takes more than 20 min. The limitation of this proposed method is that the slope must be homogeneous and isotropic and the slope angle is unique. If the slope has multiple steps with different angles, a equivalent slope angle must be determined for the application of the proposed method.

Author contributions All authors contributed to the study. The first draft of the manuscript was written by Wenlian Zhang and all authors commented on previous versions of the manuscript. The study design and conception were provided by Xiaoyun Sun and Wei Yuan. The model design, data simulation and analysis were performed by Wenlian Zhang. Ting Liu and Shenyi Jin completed some simulation and figures preparation. All authors read and approved the final manuscript.

Data availability All data needed for the study have been provided in the paper, and no other data is required.

Declarations

Conflict of interest The authors have no competing interests as defined by Springer, or other interests that might be perceived to influence the results and/or discussion reported in this paper.

References

Balmer G (1952) A general analytical solution for Mohr's envelope. American Society Test Mater 52:1269–1271

Du SG (2018) Method of equal accuracy assessment for the stability analysis of large open-pit mine slopes. Chin J Rock Mech Eng 37(06):1301–1331

Fu WX, Liao Y (2010) Non-linear shear strength reduction technique in slope stability calculation. Comput Geotech 37(3):288–298. https://doi.org/10.1016/j.compgeo.2009.11.002

Hammah RE, Yacoub TE, Corkum B, et al (2005) The shear strength reduction method for the generalized Hoek-Brown criterion. Proceedings of the 40th US Symposium on Rock Mechanics. Alaska Rocks 2005, Anchorage. Alaska.

Han LQ, Wu SC, Li ZP (2016) Study of non-proportional strength reduction method based on Hoek-Brown failure criterion. Rock Soil Mech 37(A2):690–696. https://doi.org/10.16285/j.rsm.2016.S2.088

Hoek E, Brown ET (1980) Empirical strength criterion for rock masses. J Geotech Eng Div 106(GT9):1013–1035

Hoek E, Brown ET (2019) The Hoek-Brown failure criterion and GSI – 2018 edition. J Rock Mech Geotech Eng 11(3):445–463. https://doi.org/10.1016/j.jrmge.2018.08.001

Hoek E, Carranza-Torres CT, Corkum B (2002) Hoek-Brown failure criterion-2002 edition. In: Proceedings of the Fifth North American Rock Mechanics Symposium (NARMS-TAC), University of Toronto Press, Toronto: 267–273

Krahn J (2007) Limit equilibrium, strength summation and strength reduction methods for assessing slope stability. Int J Life Cycle Assess 14(2):175–183. https://doi.org/10.1201/noe0415444019-c38

Li AJ, Merifield RS, Lyamin AV (2008) Stability charts for rock slopes based on the Hoek-Brown failure criterion. Int J Rock Mech Min Sci 45(5):689–700. https://doi.org/10.1016/j.ijrmms.2007.08.010

Li AJ, Merifield RS, Lyamin AV (2011) Effect of rock mass disturbance on the stability of rock slopes using the Hoek-Brown failure criterion. Comput Geotech 38(4):546–558. https://doi.org/10.1016/j.compgeo.2011.03.003

Liu SY, Shao LT, Li HJ (2015) Slope stability analysis using the limit equilibrium method and two finite element methods. Comput Geotech 63:291–298. https://doi.org/10.1016/j.compgeo.2014.10.008

Melkoumian N, Priest SD, Hunt SP (2009) Further development of the three-dimensional Hoek-Brown yield Criterion. Rock Mech Rock Eng 42(6):835–847. https://doi.org/10.1007/s00603-008-0022-0

Priest SD (2005) Determination of shear strength and three-dimensional yield strength for the Hoek-Brown criterion. Rock Mech Rock Eng 38(4):299–327. https://doi.org/10.1007/s00603-005-0056-5

Russo G (2008) A new rational method for calculating the GSI. Tunn Undergr Space Technol 24(1):103–111. https://doi.org/10.1016/j.tust.2008.03.002

Sari M (2019) Stability analysis of cut slopes using empirical, kinematical, numerical and limit equilibrium methods: case of old Jeddah-Mecca road (Saudi Arabia). Environ Earth Sci 78(21):621. https://doi.org/10.1007/s12665-019-8573-9

Shen JY, Karakus M (2014) Three-dimensional numerical analysis for rock slope stability using shear strength reduction method. Can Geotech J 51(2):164–172. https://doi.org/10.1139/cgj-2013-0191

Shen JY, Karakus M, Xu CS (2012) Direct expressions for linearization of shear strength envelopes given by the Generalized Hoek-Brown criterion using genetic programming. Comput Geotech 44:139–146. https://doi.org/10.1016/j.compgeo.2012.04.008

Shen JY, Karakus M, Xu CS (2013) Chart-based slope stability assessment using the generalized Hoek-Brown criterion. Int J Rock Mech Min Sci 64:210–219. https://doi.org/10.1016/j.ijrmms.2013.09.002

Song K, Yan EC, Mao W et al (2012) Determination of shear strength reduction factor for generalized Hoek-Brown criterion. Chin J Rock Mech Eng 31(1):106–112

Sukanya C, Heinz K, Katrin W (2012) A comparative study of different approaches for factor of safety calculations by shear strength reduction technique for non-linear Hoek-Brown failure criterion. Geotech Geol Eng 30(4):925–934. https://doi.org/10.1007/s10706-012-9517-2

Sun CW, Chai JR, Xu ZG et al (2016) Stability charts for rock mass slopes based on the Hoek-Brown strength reduction technique. Eng Geol 214:94–106. https://doi.org/10.1016/j.enggeo.2016.09.017

Thomas B, Radu S, Regina AK et al (2008) A Hoek-Brown criterion with intrinsic material strength factorization. Int J Rock Mech Min Sci 45(2):210–222. https://doi.org/10.1016/j.ijrmms.2007.05.003

Wei YF, Fu WX, Ye F (2021) Estimation of the equivalent Mohr-Coulomb parameters using the Hoek-Brown criterion and its application in slope analysis. Eur J Environ Civ Eng 25(4):599–617. https://doi.org/10.1080/19648189.2018.1538904

Wu SC, Jin AB, Gao YT (2006) Numerical simulation analysis on strength reduction for slope of jointed rock masses based on generalized Hoek-Brown failure criterion. Chin J Geotech Eng 28(11):1975–1980

Xu JS, Yang XL (2018) Seismic stability analysis and charts of a 3D rock slope in Hoek-Brown media. Int J Rock Mech Min Sci 112:64–76. https://doi.org/10.1016/j.ijrmms.2018.10.005

Yang XL, Yin JH (2010) Slope equivalent Mohr-Coulomb strength parameters for rock masses satisfying the Hoek-Brown criterion. Rock Mech Rock Eng 43(4):505–511. https://doi.org/10.1007/s00603-009-0044-2

Yuan W, Li JX, Li ZH et al (2020) A strength reduction method based on the generalized Hoek-Brown (GHB) criterion for rock slope stability analysis. Comput Geotech 117:103240. https://doi.org/10.1016/j.compgeo.2019.103240

Zhang WL, Sun XY, Chen Y (2022) Slope stability analysis method based on compressive strength reduction of rock mass. Rock Soil Mech 43(S2):607–615. https://doi.org/10.16285/j.rsm.2021.0170

Zhao SY, Zheng YR, Shi WM, Wang JL (2002) Analysis on safety factor of slope by strength reduction FEM. Chin J Geotech Eng 24(3):343–346

Zhao SY, Zheng YR, Zhang YF (2005) Study on slope failure criterion in strength reduction finite element method. Rock Soil Mech 26(2):332–336. https://doi.org/10.16285/j.rsm.2005.02.035

Zong QB, Xu WY (2008) Stability analysis of excavating rock slope using generalized Hoek-Brown failure criterion. Rock Soil Mech 29(11):3071–3076. https://doi.org/10.16285/j.rsm.2008.11.037